Extreme Poisson's ratios recorded in the secondary phloem of Malvaceae: a highlight on the biomechanical function of bark

Tancrède Alméras, Stéphane Corn, Anne Baranger, Arnaud Regazzi, Jonathan Barés, Romain Lehnebach, Bruno Clair

Extreme Poisson's ratios recorded in the secondary phloem of Malvaceae: a highlight on the biomechanical function of bark

Tancrède Alméras[1*], Stéphane Corn[2], Anne Baranger[1,3], Arnaud Regazzi[2], Jonathan Barés[1], Romain Lehnebach[3], Bruno Clair[1]

1: Laboratoire de Mécanique et Génie Civil, Univ Montpellier, CNRS, Montpellier, France

2: LMGC, IMT Mines Alès, Univ Montpellier, CNRS, Ales, France

3: UMR EcoFoG, AgroParisTech, CIRAD, CNRS, INRAE, Univ Antilles, Univ Guyane, Kourou, France

* Author for correspondence: tancrede.almeras@umontpellier.fr

	Orcid id	e-mail
Tancrède Alméras	0000-0002-2843-5466	tancrede.almeras@umontpellier.fr
Stéphane Corn	0000-0002-9819-0425	stephane.corn@mines-ales.fr
Anne Baranger	0000-0001-6929-6362	annebarang@gmail.com
Arnaud Regazzi	0000-0002-6070-2878	arnaud.regazzi@mines-ales.fr
Jonathan Barés	0000-0002-7345-0390	jonathan.bares@umontpellier.fr
Romain Lehnebach	0000-0001-6175-4437	romain.lehnebach@cirad.fr
Bruno Clair	0000-0002-4093-9034	bruno.clair@cnrs.fr

Running title: Extreme Poisson's ratio in secondary phloem

Highlight (30 words)

The secondary phloem of several angiosperm species has extraordinarily high Poisson's ratio, designed to convert the tangential strain due to cambial growth into a longitudinal stress with a motor function.

Abstract (193 words)

In some angiosperm species, especially in the Malvaceae family, postural control and directional growth of the stem are enabled by the mechanical interaction between the growing cambium and the secondary phloem. A key-feature of this motor mechanism is the ability to redirect the tangential stress induced in secondary phloem into a longitudinal stress enabling the control of stem orientation. Here we studied how the microstructure of the secondary phloem is optimized for this function. We measured the longitudinal-tangential Poisson's ratio and the longitudinal modulus of elasticity of secondary phloem in 22 tree species including Malvaceae and other families. We modeled the microstructure of Malvaceae secondary phloem using finite elements. The Poisson's ratio of secondary phloem from Malvaceae trees was found one to two orders of magnitude higher than for other species, reaching the highest values ever reported for a natural material. Mechanical modeling confirmed these results, and showed that parameters of the microstructure of secondary phloem are set at value optimizing this Poisson's ratio. This highlights that the specific microstructure of Malvaceae secondary phloem is designed to maximize the conversion of cambial growth pressure into a longitudinal mechanical stress enabling the directional growth.

Key-words: biomechanics, gravitropism, Malvaceae, Poisson's ratio, posture control, secondary phloem

Word count: 3710 (from introduction to acknowledgements, excluding material and methods, tables and figure legends)

Table count: 1

Figure count: 7 (all in color)

Introduction

Bark plays multiple functions in the tree, including the transport of carbohydrates, storage of reserves, defense and mechanical support (Rosell, 2019). Its mechanical role includes a "skeletal" function, i.e. a contribution to stem stiffness and strength (Niklas, 1999; Rosell and Olson, 2014). This function is particularly important in the early stages when the ratio of bark thickness to stem diameter is larger than in further stages (Lehnebach et al., 2020b; Rosell, 2016). This skeletal function is necessary to minimize the amount of bending undergone by the stem when it grows in the field of gravity or when it is exposed to external loadings such as wind. However, a skeletal system alone is not sufficient to ensure the postural control of the tree, i.e. the control of the orientation of its axes. A "motor" system (Moulia et al., 2006) is also required to restore the orientation after a major disturbance, or just to compensate for the effect of the increasing tree weight during growth (Alméras and Fournier 2009). In trees, this motor function has long been thought to be exclusively performed by wood during its maturation (Scurfield, 1973). The mechanism underlying this motor function is well described at the macroscopic level: physical and chemical processes occurring during the maturation of wood fibers induce mechanical stresses in the newly formed tissue, called "maturation stress". Their magnitude depends on the wood microstructure and chemical composition. Various hypotheses have been proposed to explain the origin of these stresses at the macromolecular level as reviewed in Gorshkova et al. (2015) and Alméras and Clair (2016). When these maturation stresses are asymmetrically distributed around the stem (e.g. in the occurrence of reaction wood on one side of the stem), they induce a bending moment that curves the stem up.

Recently, the contribution of the secondary phloem to this motor function has been demonstrated and quantified (Clair et al., 2019). In young stems of certain tree species (especially in the Malvaceae family), the inner bark rather than wood is the main motor of gravitropism and posture control (Ghislain et al., 2019a). This behavior is associated to a pronounced eccentricity of the secondary growth (Ghislain et al., 2019a), and to a specific anatomy of secondary phloem, where phloem fibers form a "trellis" structure (Fig. 1) : fibers wave in the longitudinal-tangential plane and are laterally connected (Angyalossy et al., 2016; Böhlmann, 1971; Zajączkowska and Kozakiewicz, 2016). A mechanism by which tensile longitudinal stress is set in secondary phloem during growth has been proposed (Clair et al., 2019) (Fig. 1). The expansion of growing tissues located between wood and bark during cambial growth generates a mechanical stress in the radial direction σ_R. This stress pushes the secondary phloem outward, expanding it circumferentially and thus inducing a tangential stretching strain in it, ε_T. Because of the trellis organization of the secondary phloem's fibers, this tangential tension is redirected into the longitudinal direction, creating a longitudinal tensile stress σ_L.

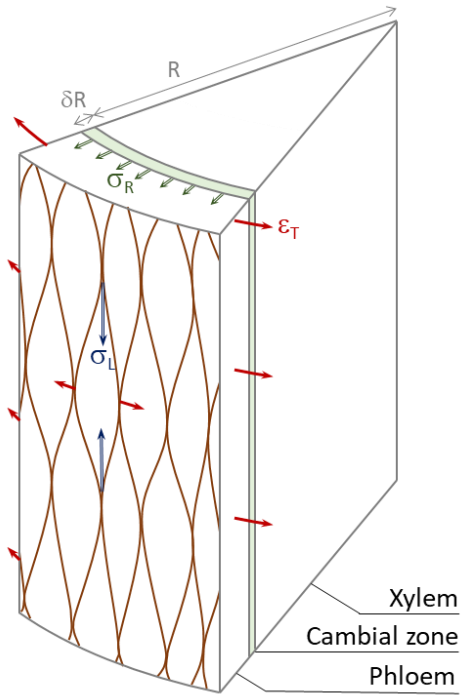

Fig. 1: *Mechanical interaction between growing tissues and secondary phloem of Malvaceae. Growing tissues in the cambial zone generate a radial stress σ_R at the interface with secondary phloem. This radial stress cause tangential extension of secondary phloem ε_T. This tangential extension induces a longitudinal tension σ_L thanks to the trellis structure of the fibers in the secondary phloem.*

Therefore, the cambial growth sets the secondary phloem in a state of longitudinal tension, as has been show experimentally (Lehnebach et al., 2020b). When eccentric growth occurs, a higher longitudinal tension is induced on the side of the preferential growth compared to the opposite side. This asymmetry in tension generates a bending moment that leads to a change in curvature of the stem.

The redirection of the tangential stress into the longitudinal direction is the key feature of this mechanism of postural control based on secondary phloem. From an engineering point of view, the fact that a material contracts in one direction when it is stretched in the orthogonal direction is called the Poisson's effect. It is quantified by the Poisson's ratio, denoted ν_{XY}. This is the ratio between the negative strain (i.e. contraction) induced in direction Y and the positive strain (i.e. stretching) in direction X that caused it. In isotropic materials (i.e. materials having the same properties in all directions), the Poisson's ratio is necessarily lower than 0.5. In anisotropic materials, it can be larger than 0.5, and it is affected by the degree of anisotropy, being physically bounded as follows:

$\nu_{XY} < \sqrt{E_X/E_Y}$., where E_X and E_Y are the Young's moduli of the material in directions X and Y, respectively.

The Poisson's ratio quantifies the intensity of kinematic coupling between two directions. It is worth noting that ν_{XY} (the amount of contraction induced in direction Y when stretching the material in direction X) and ν_{YX} (the amount of contraction induced in direction X when stretching the material in direction Y) are different, and related by $\nu_{YX}/\nu_{XY} = E_Y/E_X$ for an orthotropic material. It can be shown that the ratio between the longitudinal stress σ_L induced in the secondary phloem and the radial stress σ_R that caused it is proportional to the longitudinal-tangential Poisson's ratio (ν_{LT}).

The aim of the present study is to quantify to which extent the secondary phloem of species which use it as a motor of gravitropic movements is mechanically adapted to this function. To do so we measured the elastic properties (longitudinal elastic modulus and longitudinal-tangential Poisson's ratio) of secondary phloem from young branches of a large diversity of tropical species including both Malvaceae and other botanical families. We found that this latter family exhibited extraordinarily high Poisson's ratio. Then, based on the trellis structure of Malvaceae secondary phloem, we built a parameterized finite element model designed to quantify the influence of the main microstructural features of the secondary phloem on its functional properties. This model aims at (*i*) validating the experimental results, by demonstrating that the actual microstructure of Malvaceae can result in such large Poisson's ratios, (*ii*) studying the optimality of the microstructure with respect to generating large Poisson's ratio. For objective (*i*), realistic values of parameters are needed, so we did measurements of secondary phloem microstructure and refer to them when commenting the simulation results. For objective (*ii*), we will use a larger range of parameters, representing all possible microstructure configurations, even configurations that are not found in nature. Doing so, we show that the actual microstructure of secondary phloem in Malvaceae leads to maximizing the Poisson's ratio.

Material and Methods

Plant material

Large diversity of tree species and secondary phloem structures was attained by collecting plant material from the hyperdiverse forest of French Guiana at the Nouragues experimental research station (4°05'N, 52°40'W). This station has facilities to access to canopy, allowing to collect small branches on mature identified trees. We sampled 22 species belonging to different botanical families, among which 4 belonged to the Malvaceae (see Suppl. Mat. Table S1 for the full list of species). For each species, we collected 5 branches with basal diameter between 1 and 2 cm. For the anatomical

study, the branches were cut into a 2 cm long segments kept in 50 % ethanol, while for tensile tests 10 cm long segments were cut and kept immersed in distilled water at 5°C.

Secondary phloem's mechanical properties

The Young's modulus of secondary phloem and its Poisson's ratio were determined using tensile tests. They were performed on strips of secondary phloem taken from the branch segments. The strips were approximately 5 cm long (in the longitudinal direction), 4 mm wide (in the tangential direction) and between 1 and 2 mm thick (in the radial direction) depending on the specimen (Fig. 2). They were mounted between the jaws of an MTS 1/ME testing machine equipped with a 500 N load cell, and stretched at a constant speed of 0.01 mm/s. During the loading process, the outward surface of the sample was imaged with a digital camera (svs-vistek hr16070MFLGEC) having a CCD of 4864 x 3232 pixels and equipped with a telecentric lens (Myutron LSTL10H-F) with focal length of 113.3 mm. The distance between the camera and the specimen was 343 mm, and the field of view of the camera was 35.8 x 23.8 mm, yielding images with resolution of 116 pixel/mm.

Then the displacement field of the specimen surface was computed by means of a digital image correlation (DIC) algorithm dedicated to large deformations and inhomogeneous patterns (Vu et al., 2019). This DIC algorithm computes the displacement field both in the longitudinal and in the tangential directions over the surface of the specimen as a function of the loading. An illustration of such displacement field is shown in Fig. 2 for several points located along nine parallel lines. Strain fields were derived from the displacement fields. For each sample, the mean strain was computed on a central area of the specimen, excluding the boundaries. The longitudinal elastic modulus was computed as the slope of the longitudinal stress-strain curve in its linear part (see Fig. 2). The LT Poisson's ratio was computed as the opposite of ratio between tangential strain and longitudinal strain. In many instances, the Poisson's ratio appeared strain-dependent (see Fig. 2), even in the linear domain of the stress-strain curve. In this case, a mean value was computed. In four instances, the stress-strain curve did not contain a satisfying linear domain. These tests were removed from the analysis so that the average value of these species was computed on four specimens.

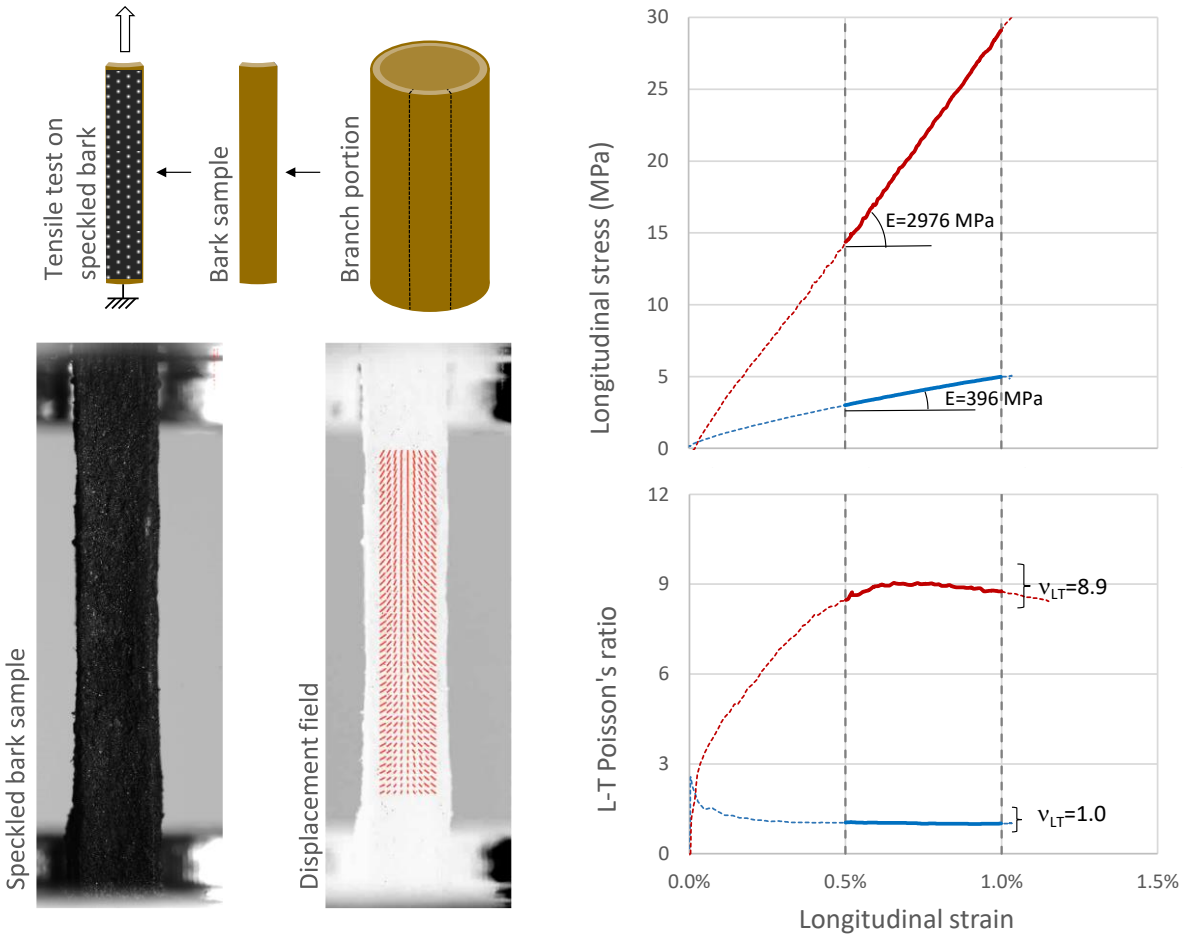

Fig. 2. *Method for measuring longitudinal elastic modulus and Poisson's ratio on bark specimens. (Top left) a tangential strip of bark is taken from a branch portions and a speckled pattern is applied on it. (Bottom left) the specimen is imaged during the tensile test, and the displacement field is computed using digital image correlation. (Right) longitudinal and tangential strains are derived from it, and used to compute the elastic modulus and Poisson's ratio. Stress-strain curve and Poisson's ratio-strain curve are shown for two examples: a specimen with low elastic modulus and Poisson's ratio, and a Malvaceae specimen with large elastic modulus of Poisson's ratio.*

Bark anatomy

The organization of phloem fibers in the transverse and longitudinal-tangential planes of each species was described under an optical microscope. For this purpose, thin sections (5-6 µm) in the transverse and LT planes were prepared after embedding the samples in paraffin and staining them with FASGA (safranin + Alcian blue). For LT section, several sections from outer bark to cambium were prepared. For each species, 3 segments were observed to account for the within-species variability. Quantitative measurements, namely the percent fiber content and the aspect ratio, were performed to feed the

finite element model (see next section) on 2 Malvaceae species, *L. rugosa* and *Q. spatulata*, with the image analysis software ImageJ (Schneider et al., 2012).

Finite element analysis

A finite element model was developed using Comsol Multiphysics® software in order to investigate the way the elastic constants of the secondary phloem are affected by the geometric parameters characterizing the structure of the fibrous trellis. A periodic microstructure inspired by the trellis pattern of phloem tissue was devised by considering both parenchyma and fibers (Fig. 3). Assuming two-directional periodicity in the LT plane of this microstructure, the finite element model was simplified to a rectangular representative unit cell as described in Figure 3B. The main geometrical features of this cell were described with a set of three parameters: the fiber volume fraction φ, the aspect ratio γ of the length of the cell L over its width T, and the relative length of fiber lateral connections τ which is the ratio of the total length of joined fibers $2L_c$ over the length of the cell L. Following the conclusions of a preliminary study, parameter τ was set at a fixed value of 0.3, while other parameters were varied during the parametric study. Parameter φ directly indicates the abundance of fibers relative to parenchyma. The aspect ratio γ indicates the degree of alignment of fibers: a high aspect ratio corresponds to fibers aligned with the L direction.

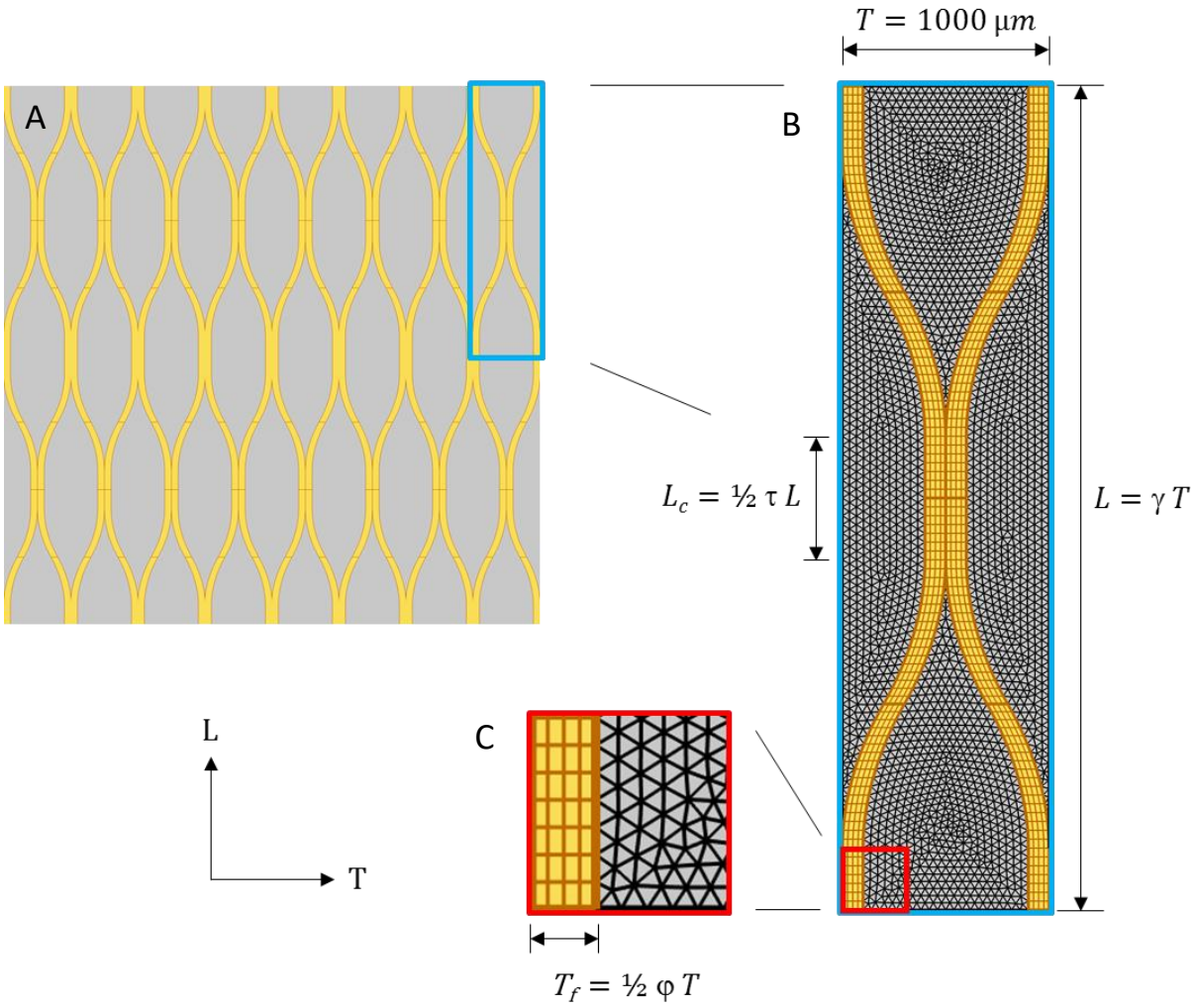

198

199 ***Fig 3.*** *Finite element model of the unit cell of a trellis microstructure and the corresponding set of*
200 *dimensional parameters. Fibers are colored in yellow and parenchyma tissues in grey. Fiber and*
201 *parenchyma are assumed perfectly bonded. A: abstraction of the geometry of the trellis structure. B:*
202 *unit cell of which the structure is a periodic repetition. C: finite-element mesh. The geometry of the*
203 *trellis is defined by 3 dimensionless parameters: the aspect ratio γ, the fiber fraction φ and the*
204 *connection length τ.*

205 The mechanical behaviors of both parenchyma and fibers were assumed linear and elastic. Fibers were
206 considered transversely isotropic, the plane of isotropy being normal to the axis of fibers, and
207 parenchyma were considered isotropic. The elastic constants of each material are listed in Table 1.
208 Elastic constants of the fibers were set at values consistent with wood properties (Forest Products
209 Laboratory, 2010). The modulus of elasticity of parenchyma was defined as the ratio of the longitudinal
210 elastic modulus of fibers over 10^{μ} where μ is the stiffness contrast parameter, that was varied during
211 the parametric study.

212 *Table 1: Elastic components of secondary phloem's constituents used in the finite element model*

Elastic components	*Fibers*	*Parenchyma*
Tensile modulus	$E_L^f = 20$ GPa	$E^p = E_L^f/10^\mu$
	$E_T^f = E_R^f = 1.6$ GPa	
Shear modulus	$G_{LT}^f = 1.8$ GPa	$G^p = E^p/\left(2(1+\nu^p)\right)$
	$G_{TR}^f = E_T^f/\left(2\left(1+\nu_{TR}^f\right)\right)$	
Poisson's ratio	$\nu_{LT}^f = 0.45$	$\nu^p = 0.3$
	$\nu_{TR}^f = \nu_{RT}^f = 0.30$	

The finite element mesh of the unit cell was made of 3D prismatic elements obtained from the extrusion (depth of $T/10$) of a 2D mesh consisting of quadrangular and triangular elements as illustrated in Figure 3C. A mesh convergence study has been carried out leading to a maximum element size of $L/100$, resulting in a 11,040 elements mesh.

In order to assess the average elastic properties of the homogenized material over the large repetitive structure of the trellis, cell periodicity conditions were implemented. It consists in creating three periodic pairs of boundary conditions on the outer boundaries of the unit cell (one for each space direction in the frame of reference). The boundary conditions are governed by the following displacement continuity relation: $u_{dst} - u_{src} = \acute{\varepsilon}(X_{dst} - X_{src})$. In this relation, u, X and $\acute{\varepsilon} = \left(\int_V \varepsilon dV\right)/V$ are respectively the displacement field, the coordinates and the average strain of the source (src) and destination (dst) boundaries. For each pair, the representative volume element is subjected to a unit strain in a given direction of the frame of reference while the other strain components of the pair are kept equal to zero. Then the average stress $\acute{\sigma} = \left(\int_V \sigma dV\right)/V$ is evaluated allowing the determination of the elasticity tensor $\acute{C}$ for the equivalent homogenized material with respect to the relation $\acute{\sigma} = \acute{C}.\acute{\varepsilon}$.

The behavior of the homogenized material was also compared to the behavior of a composite made of parallel fibers (without lateral connections), for which E_L corresponds to the Voigt bound (parallel association between fibers and parenchyma) and E_T corresponds to the Reuss bound (series association between fibers and parenchyma).

For the parametric study of the model, the fiber volume fraction φ and the aspect ratio γ were varied between 0.1 and 0.9 and between 1 and 20, respectively. The relative length of fiber lateral connections τ and elastic constants of the fibers were kept at fixed values. The stiffness contrast parameter μ was varied between 1 and 6.

Results

Mechanical properties

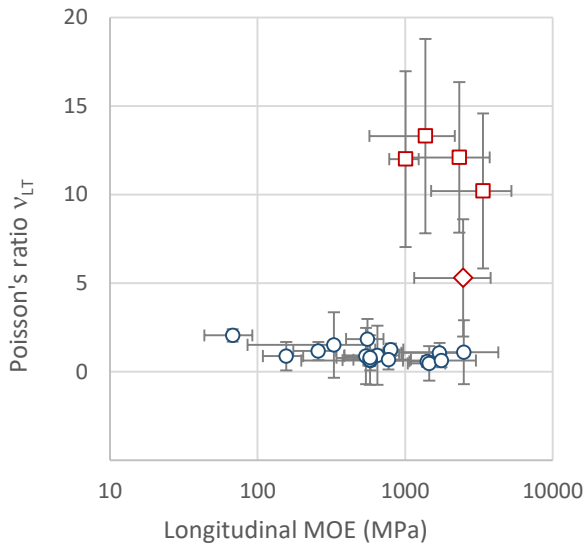

Fig 4. *Mean elastic properties of the secondary phloem: Poisson's ratio ν_{LT}, as a function of the longitudinal modulus of elasticity, E_L for different species. For each species data are averaged over 5 specimens. The standard deviations are given for both ν_{LT} and E_L by grey vertical and horizontal lines, respectively. The red squares specifically show the species from the Malvaceae family. The red diamond is the Annonaceae species. X-axis is in logarithmic scales.*

The stress-strain curves and Poisson's ratio-strain curves of all specimens are provided as supplementary material (see suppl. mat. Fig. S4). Figure 4 summarizes the results for all studied species (mean Poisson's ratio, mean modulus of elasticity and their standard deviation). For most species, the Poisson's ratio ν_{LT} ranges between 0.5 and 2. For the species from the Malvaecae family, the Poisson's ratio is one order of magnitude higher, ranging between 10 and 13. One species which does not belong to the Malvaceae family (*U. rufescens,* Annonaceae) also has a high Poisson's ratio (value near 5, indicated by a red diamond). This family is anatomically and functionally similar to Malvaceae, with a similar secondary phloem consisting of a fiber trellis structure (Fig. 5) and a similar reaction wood made of parenchyma cells (Ghislain et al., 2019b).

The elastic modulus of secondary phloem in its longitudinal direction spans over more than one order of magnitude, ranging from 70 MPa to more than 3000 MPa. Within-species variability is rather high, but small compared to between-species variability (R^2=0.59, $p<10^{-6}$). Species from the Malvaceae family, as well as *U. rufescens* (Annonaceae), are among the highest elastic moduli (between 1000 MPa and 3000 MPa). This shows that their high Poisson's ratios are associated with high elastic moduli.

However, the reciprocal is not true, i.e. high elastic moduli are not always associated to high Poisson's ratio (five species have elastic modulus larger than 1000 MPa but Poisson's ratio lower than 2, Fig. 4).

Anatomy

Transverse sections show the layered organization of bark, with secondary phloem on the inner side and suber on the outer side. The thickness of secondary phloem varies between species, but is always much larger than the suber layer. The analysis of the anatomical sections showed that all species with a Poisson's ratio higher than 5 exhibited a typical organization of fibers in their inner bark (Fig. 5-A,H,I,J,K). Namely, in the transverse section, flame-shaped areas of fibers are separated by dilatation parenchyma. In the L-T section, large fiber bundles are undulating and are physically connected in the tangential direction, forming a typical "trellis" structure, the space between them being filled with dilated parenchyma (Angyalossy et al., 2016; Böhlmann, 1971; Zajączkowska and Kozakiewicz, 2016). This was the case for the 4 species of the Malvaceae family (Fig. 5-H,I,J,K) as well as for the Annonaceae (Fig. 5-A). In the other species, fibers were either present (*P. apiculatum, C. aromatica, E. falcata, T. surinamensis, V. michelii, E. coffeifolia, L. crenata, H. alchorneoides*) or absent (*L. aculeata, I. fastuosa, S. polyphylla, C. surinamensis, N. guianensis, N. floribunda, S. acreanum, L. procera, C. argenteum*), but when present they were not organized as a trellis, except for one species (*E. falcata,* Fig. 5-E) which had fibers laterally connected (consistently with Lehnebach et al., 2020) although its Poisson's ratio was found lower than 5. Interestingly, this specie also exhibits a band of heavily lignified sclerites (suppl. mat. Fig. S5), which is absent in Malvaeae and Annonaceae. This feature very likely impedes tangential strains and thus limits the Poisson's effect.

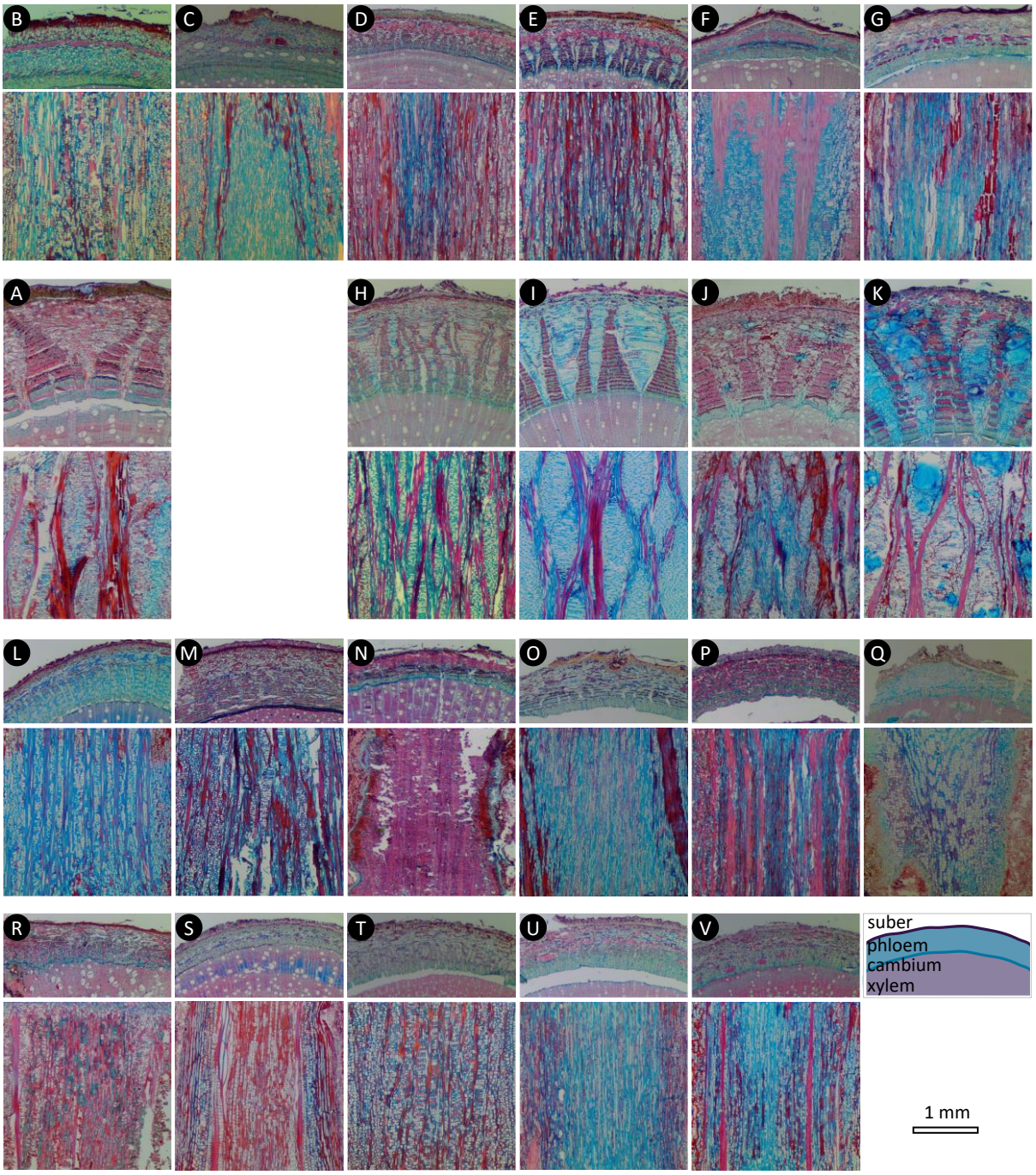

Fig. 5. *Cross sections (top) and longitudinal-tangential sections (bottom) of studied species. Cross sections were performed on branch segments including wood. Bark (phloem + suber) is presented on the upper side of the images and xylem on the lower side. (A) Unonopsis rufescens (*Annonaceae*); (B) Lacmellea aculeata (*Apocynaceae*); (C) Protium apiculatum (*Burseraceae*); (D) Crudia aromatica (*Fabaceae*); (E) Eperua falcata (*Fabaceae*); (F) Inga fastuosa (*Fabaceae*); (G) Swartzia polyphylla (*Fabaceae*); (H) Lueheopsis rugosa (*Malvaceae*); (I) Quararibea spatulata (*Malvaceae*); (J) Sterculia frondosa (*Malvaceae*); (K) Sterculia villifera (*Malvaceae*); (L) Carapa suninamensis (*Meliaceae*); (M) Trichilia surinamensis (*Meliaceae*); (N) Naucleopsis guianensis (*Moraceae*); (O) Virola michelii*

*(*Myristicaceae*); (P) Eugenia coffeifolia (*Myrtaceae*); (Q) Neea floribunda (*Nyctaginaceae*); (R) Lacunaria crenata (*Ochnaceae*); (S) Hieronyma alchorneoides (*Phyllanthaceae*); (T) Stenostomum acreanum (*Rubiaceae*); (U) Laetia procera (*Salicaceae*); (V) Chrysophyllum argenteum (*Sapotaceae*). Scale bar = 1 mm.*

The quantitative analysis of the anatomical sections was made difficult by the heterogeneity of the structure of the secondary phloem. However, for two species (*L. rugosa* and *Q. spatulata*), the quality of the microscopic sections allowed quantitative estimations of the geometric parameters characterizing the trellis, which were then used as inputs in the finite-element model. The mean fiber content was estimated as 34 % (range 31 %-37 %) for *L. rugosa* and 28 % (range 23 %-36 %) for *Q. spatulata*. The mean aspect ratio of the elementary patterns (as defined in section "finite element analysis") was estimated as 6.4 (range 5.2-7.4) for *L. rugosa* and 3.8 (range 2.9-4.6) for *Q. spatulata*. Visual assessment of the other sections showed that these parameters were within the same range for the other Malvaceae species.

Parametric study of elastic constants

The finite element model allows to compute how the elastic constants of secondary phloem depend on the geometrical parameters characterizing the structure of the fibrous trellis. Results for E_L and E_T are shown in figure 6. Each figure shows how an elastic constant varies as a function of the fiber fraction φ and the aspect ratio γ, for a given value of the stiffness contrast parameter μ. Results are illustrated for two contrasted values of μ (results for other values of μ are provided as supplementary material Figs. S1 and S2).

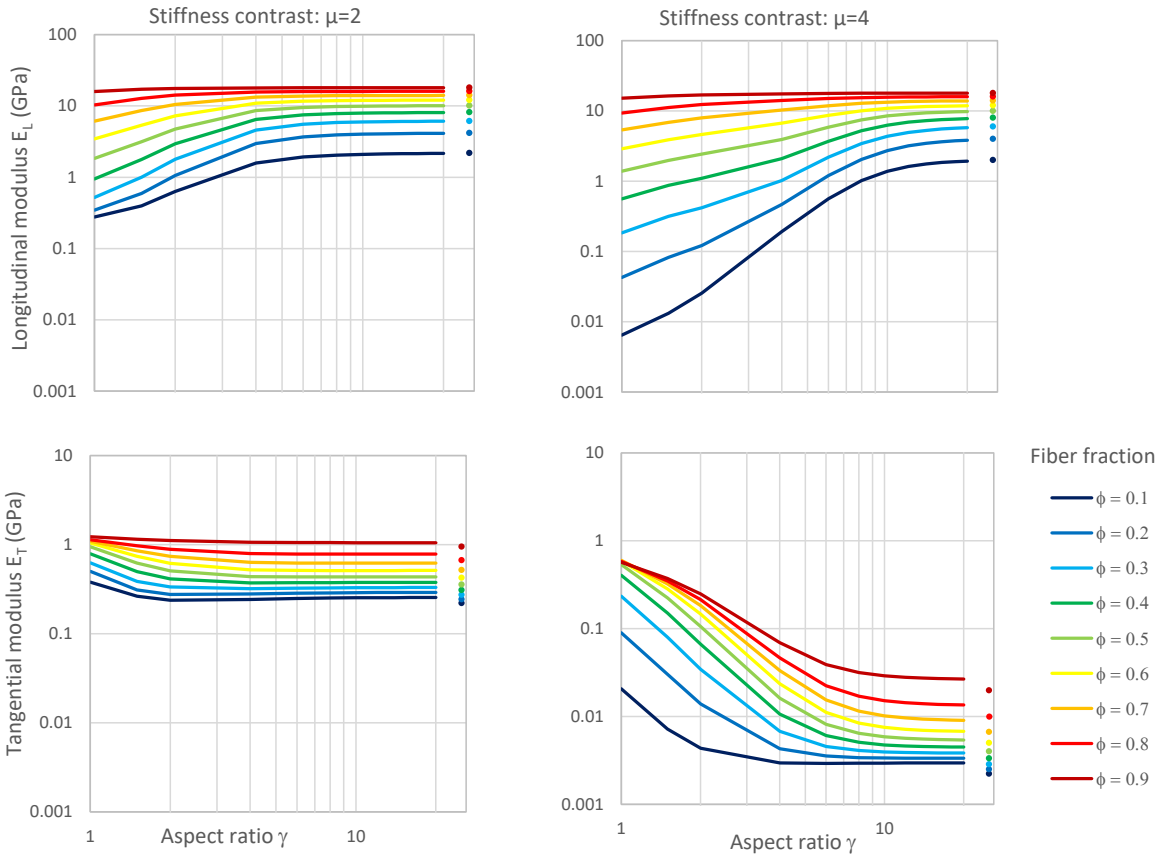

311

312 ***Fig. 6.*** *Parametric finite element modelling of the modulus of elasticity as function of the aspect ratio*
313 *γ for several values of fiber fraction φ, for two different values of the stiffness contrast parameter μ*
314 *(results for other values of μ are provided as supplementary material Fig. S1 and S2). Top: longitudinal*
315 *modulus E_L, dots are the results obtained using a parallel model (Voigt's bound). Bottom: tangential*
316 *modulus E_T, dots are the results obtained using a series model (Reuss's bound).*

317 As expected, E_L always increases as a function of the fiber fraction φ, because fibers are several orders
318 of magnitude stiffer than parenchyma. E_L decreases as a function of the stiffness contrast parameter
319 μ consistently with the fact that the elastic modulus of parenchyma decreases with μ. E_L increases as
320 a function of the aspect ratio γ, because γ determines the degree of alignment of fibers in the
321 longitudinal direction (a higher aspect ratio makes the fibers straighter). When the fiber fraction φ is
322 high, E_L is weakly sensitive to variations of γ and μ, and tends towards the elastic modulus of fibers.
323 The lower the fiber fraction φ, the more E_L is sensitive to the stiffness contrast parameter μ and the
324 aspect ratio γ. For high values of the aspect ratio γ, the elastic modulus of secondary phloem E_L tends
325 towards the Voigt bound, i.e. the value obtained if fibers and parenchyma are organized in parallel
326 (not laterally connected). In this case, E_L is close to a simple rule of mixture of the elastic moduli of the
327 components: $E_L = \varphi E_L^f + (1-\varphi)E^p$. As the elastic modulus of parenchyma is several orders of

magnitude lower than that of fibers, the contribution from parenchyma is always negligible, so that E_L mainly depends on φ and its sensitivity to μ is very low (see Suppl. Mat. Fig. S1).

Results for the tangential elastic modulus E_T are shown in figure 6 (bottom) and in suppl. mat. (Fig. S2). Just as for E_L, E_T expectedly increases as a function of the fiber fraction φ and decreases as a function of the stiffness contrast parameter μ. Contrary to E_L, E_T decreases as a function of the aspect ratio γ. Since γ determines the alignment of fibers with the longitudinal direction, low values of γ correspond to fibers oriented more diagonally and therefore more efficient in reinforcing E_T. The value of E_T is very sensitive to the stiffness contrast parameter μ, much more than for E_L. Thus, the behavior of the secondary phloem in the tangential direction strongly depends on the properties of the parenchyma. The association between fibers and parenchyma is closer from the Reuss's bound in this direction, i.e. a "series" model, where $1/E_T = \varphi/E_T^f + (1-\varphi)/E^p$. Hence, the behavior of the most compliant component is dominating. However, even for higher values of γ, E_T is significantly higher than predicted by the series model. This means that the lateral connections between fibers efficiently reinforce the tangential direction, even when fibers orientation is close to the longitudinal direction.

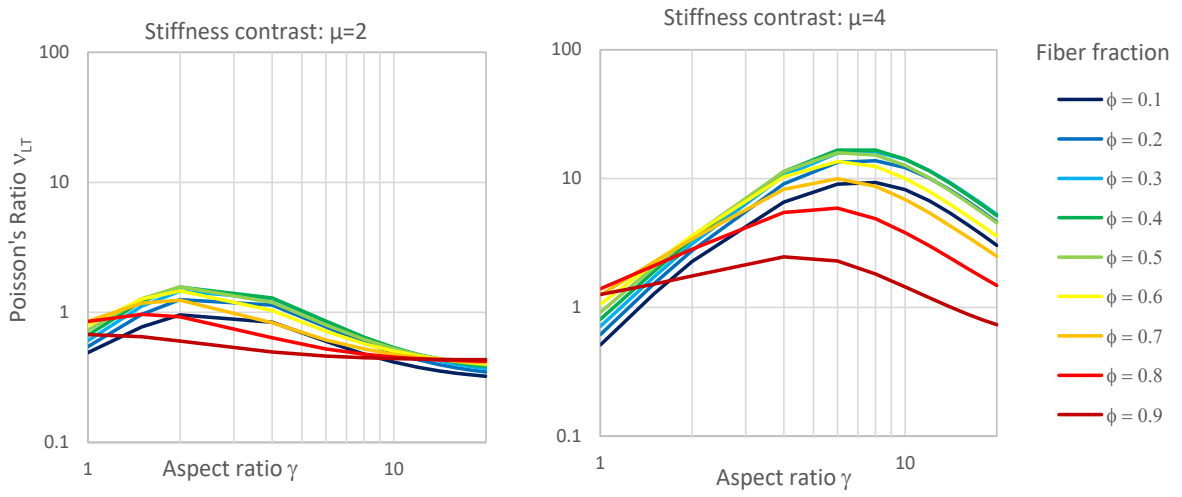

Fig. 7. *Parametric finite element modelling of the Poisson's ratio ν_{LT} as a function of the aspect ratio γ for several values of fiber fraction φ, for two different values of the stiffness contrast parameter μ (results for other values of μ are provided as supplementary material Fig. S3).*

Results of the Poisson's ratio ν_{LT} are shown in figure 7 (top) and in suppl. mat. (Fig. S3). Variations of the Poisson's ratio as a function of the geometrical parameters are non-trivial and non-monotonous. ν_{LT} presents an optimum both in γ and φ. The magnitude of the Poisson's ratio ν_{LT} is very sensitive to the value of the stiffness contrast parameter μ: high values of the Poisson's ratio are obtained when μ is large, i.e. when the parenchyma is compliant. For $\mu = 4$, the maximal value of the Poisson's ratio is 16 and is obtained when $\gamma = 6$ and $\varphi = 0.4$. These values can be compared to the experimental data,

were ν_{LT} ranges between 10 and 13, γ between 3 and 7 and φ between 0.2 and 0.4. Finite element modeling validates the experimental measurement and evidences the ability of such trellis structure to produce unexpectedly high Poisson's ratios. These values of Poisson's ratios and geometrical parameters are similar to the experimental values and suggest that $\mu = 4$ is a good estimation of actual stiffness contrast parameter. Moreover, for this value of μ and for experimental values of the geometrical parameter, a good agreement is also obtained between the computed longitudinal elastic modulus (ranging between 500 MPa and 3000 MPa) and its experimental range of variation (between 1000 and 3000 MPa).

Discussion

The Poisson's ratio values found in our experimental study on inner barks from the Malvaceae family are extraordinarily high, ranging from 10 to 13. In comparison, for isotropic materials (i.e. materials with the same properties in all directions, such as for instance glass, metals, rubber...) this parameter is physically limited to 0.5, and most of the materials are below this limit (Greaves et al., 2011). However, this physical limit does not hold for anisotropic materials, where larger values are frequently reported. For instance, Lethbridge et al. (2010) reported extreme values up to 10 for some crystalline materials. Although plant tissues are often anisotropic, it has never been reported such high values for their constitutive materials. Poisson's ratios have been measured to be approximately 0.5 for cork (Ashby and Gibson, 1997), 0.35 for onion epidermal tissues (Kim et al., 2015) and between 0.1 and 0.5 for inner tissues of different plant organs (Hejnowicz and Sievers, 1995). Even in a highly anisotropic material like wood, the typical Poisson's ratio ranges between 0.3 and 0.6 depending on the species (Ando et al., 2018; Ashby and Gibson, 1997; Forest Products Laboratory, 2010). For outer tissues of different plant organs, the largest values reported in the literature range between 0.5 and 2 (Hejnowicz and Sievers, 1995), consistently with our results on secondary phloem of non-Malvaeace species. Much larger values can be found in fiber-based man-made materials, up to 13 for the apparent Poisson's ratio of yarns (Takatera et al., 2017; Wang et al., 2018) and 14 for laminate composites (Peel, 2005). To the best of our knowledge, this is the highest value measured so far in a natural material.

Theoretical studies show that the Poisson's ratio tends towards an infinite value for materials such as honeycombs (Masters and Evans, 1996) or laminate composites (Peel, 2005) with specific microstructures. For honeycombs, this happens when the microstructure is made of flat hexagons (Masters and Evans, 1996). This latter architecture is very close from the phloem fiber organization in Malvaceae as studied in the present work (Fig. 5). For laminate composites, Peel (2005) showed that high Poisson's ratio values can be obtained for large stiffness contrast between the matrix and the fibers. Our finite element simulations show that this large stiffness contrast is also a necessary condition to obtain a high Poisson's ratio for the type of microstructure we studied. In laminate composites, the Poisson's ratio depends also on the ply orientation with respect to the frame of reference. This dependence is non-monotonous so that there is an optimal angle at which the Poisson's ratio is maximized. This optimal angle is lower when the stiffness contrast parameter is higher (Peel, 2005). In our study, we evidenced analogous results regarding the dependence of the Poisson's ratio to the stiffness contrast and the fiber aspect ratio.

In the inner bark, our simulations show that reaching a high Poisson's ratio requires compliant parenchyma. An elastic moduli ratio between parenchyma and fibers close to 10^{-4} is necessary to reach

the value observed in Malvaceae species. This implies that the order of magnitude of the elastic modulus of parenchyma should be of about few MPa. This is consistent with values reported for apple parenchyma (Videcoq et al., 2017), and in the lower range of values usually reported for parenchyma (Niklas, 1992). By assuming a value of 10^{-4} for the stiffness contrast parameter, we obtained a close agreement between simulations and experiments, i.e. elastic properties simulated for the measured geometric parameters were consistent with experimentally measured longitudinal elastic modulus and longitudinal-tangential Poisson's ratio. Actually, a better agreement could hardly be expected because (1) the geometry we assumed is an abstraction of the real geometry of the fiber network (compare Fig. 3 and 5), and (2), the elastic properties of fibers were set at a reasonable value rather than directly measured. This agreement confirms the ability of the phloem composite material to produce exceptionally high Poisson's ratio thanks to the lateral connections between the fibers. As shown by the parametric study and the comparison with the Voigt and Reuss bounds (Fig. 6), these lateral connections only slightly reduce the longitudinal elastic modulus, but markedly increase the tangential elastic modulus. The estimation of the tangential elastic modulus is an interesting byproduct of the simulations, since direct measurement of this properties is technically challenging. Indeed, tangential strips of bark are curved, so that tensile tests are not directly feasible on this material.

In conclusion, our experimental measurements showed that Malvaceae secondary phloem has extremely high Poisson's ratio values, much larger than for other botanical families, and thus much over the highest values ever reported for a natural material. We modeled its microstructure and showed that a material comprised of a mesh of undulating fibers laterally connected inside a matrix of a much softer material, can indeed lead to such high Poisson's ratio. We studied the dependence of the elastic modulus and Poisson's ratio to variations of the geometric parameters characterizing the fiber network (fiber content and aspect ratio of an elementary volume), and predicted that, contrary to the elastic modulus, the Poisson's ratio presented an optimum with respect to these geometrical parameters. Comparison with geometric parameters evaluated experimentally showed that the real microstructure of Malvaceae secondary phloem is found to be close to the predicted optimal geometry, and its Poisson's ratio is close to that predicted by the model. The longitudinal-tangential Poisson's ratio is the parameter directly controlling the conversion of the radial stress imposed by growing cambial tissues into a longitudinal stress in secondary phloem. We infer that Malvaceae secondary phloem is designed to maximize the longitudinal stress indirectly generated by cambial growth. This longitudinal stress in secondary phloem is at the origin of posture control in this family: when asymmetrically distributed around the periphery because of eccentric radial growth, it generates a bending moment that changes stem curvature and/or counteracts the bending moment generated by the increase in stem mass. The motor power of this mechanism is provided by cambial growth

pressure, which is directly related to turgor pressure (Lockhart, 1965). Two kinds of motors of postural control are usually considered in plants (Moulia et al. 2006): those based on turgor pressure and differential growth and those based on the physical-chemical changes occurring in wood cells walls during their maturation. The formers are usually found in herbaceous stems and non-lignified organs, while the latter are found in lignified stems for which larger mechanical stress are needed. Here we found a third kind of mechanism, based on turgor pressure and differential growth of the cambial tissues, but suitable for bending lignified stems. This is made possible by the smart organization of secondary phloem, yielding a very high Poisson's ratio so that the intensity of longitudinal stress generated by the growth pressure is larger than the growth pressure itself. This mechanism of posture control differs from that of most other woody species, in which wood maturation is the motor of posture control (Alméras and Clair, 2016; Alméras and Fournier, 2009). Our previous experimental works (Ghislain et al., 2019a) showed that these two mechanisms have similar efficiency in this function for young stems. Our previous theoretical works (Alméras and Fournier, 2009) showed that, for the mechanisms based on wood maturation, the performance of the motor function tends to decrease with stem size. Further studies should investigate how the performance of the mechanism based on secondary phloem changes with stem size, to better understand and compare the adaptive value of these two divergent mechanisms.

Acknowledgements

The authors would like to thank Jonathan Prunier and Sébastien Levionnois (EcoFoG laboratory) for their assistance with fieldwork, Vincent Huon and Azza Saad (LMGC laboratory) for their assistance with mechanical measurements, Maryline Harroué and Julien Ruelle (SILVATECH facility, SILVA laboratory) for their help with anatomical cuts.

This work is part of the 'MechaBark' research project and sampling was performed at the CNRS Nouragues research field station, all funded by the French National Research Agency (CEBA ANR-10-LABX-25-01; NUMEV ANR-10-LABX-20; AnaEE France ANR-11-INBS-0001).

Authors contributions

TA and BC initiated and supervised the study.
TA, AB, BC and RL sampled the plant material.
AB, JB and RL carried out the mechanical measurements.
SC and AR did the finite-element modeling and simulations.

TA wrote initial draft. All authors contributed to analyze the data and write the manuscript. All the authors reviewed and edited the paper and approved the final version.

Data availability

Data are available at the following URL: https://doi.org/10.5281/zenodo.6673634

References

Alméras, T., Clair, B., 2016. Critical review on the mechanisms of maturation stress generation in trees. J. R. Soc. Interface 13, 20160550. https://doi.org/10.1098/rsif.2016.0550

Alméras, T., Fournier, M., 2009. Biomechanical design and long-term stability of trees: Morphological and wood traits involved in the balance between weight increase and the gravitropic reaction. J. Theor. Biol. 256, 370–381. https://doi.org/10.1016/j.jtbi.2008.10.011

Ando, K., Mizutani, M., Toba, K., Yamamoto, H., 2018. Dependence of Poisson's ratio and Young's modulus on microfibril angle (MFA) in wood. Holzforschung 72, 321–327. https://doi.org/10.1515/hf-2017-0091

Angyalossy, V., Pace, M.R., Evert, R.F., Marcati, C.R., Oskolski, A.A., Terrazas, T., Kotina, E., Lens, F., Mazzoni-Viveiros, S.C., Angeles, G., Machado, S.R., Crivellaro, A., Rao, K.S., Junikka, L., Nikolaeva, N., Baas, P., 2016. IAWA List of Microscopic Bark Features. IAWA J. 37, 517–615. https://doi.org/10.1163/22941932-20160151

Archer, R.R., 1987. Growth Stresses and Strains in Trees. Springer-Verlag, Berlin, Heidelberg.

Ashby, M.F., Gibson, L.J., 1997. Cellular solids: structure and properties. Press Syndicate of the University of Cambridge, Cambridge, UK.

Böhlmann, D., 1971. Zugbast bei *Tilia cordata* Mill. Holzforschung 25, 1–4. https://doi.org/10.1515/hfsg.1971.25.1.1

Clair, B., Ghislain, B., Prunier, J., Lehnebach, R., Beauchêne, J., Alméras, T., 2019. Mechanical contribution of secondary phloem to postural control in trees: the bark side of the force. New Phytol. 221, 209–217. https://doi.org/10.1111/nph.15375

Forest Products Laboratory, 2010. Wood handbook: wood as an engineering material.

Ghislain, B., Alméras, T., Prunier, J., Clair, B., 2019a. Contributions of bark and tension wood and role of the G-layer lignification in the gravitropic movements of 21 tropical tree species. Ann. For. Sci. 76, 107. https://doi.org/10.1007/s13595-019-0899-7

Ghislain, B., Engel, J., Clair, B., 2019b. Diversity of anatomical structure of tension wood among 242 tropical tree species. IAWA J. 40, 765–784. https://doi.org/10.1163/22941932-40190257

493 Gorshkova, T., Mokshina, N., Chernova, T., Ibragimova, N., Salnikov, V., Mikshina, P., Tryfona, T.,
494 Banasiak, A., Immerzeel, P., Dupree, P., Mellerowicz, E.J., 2015. Aspen tension wood fibers
495 contain β-(1→4)-galactans and acidic arabinogalactans retained by cellulose microfibrils in
496 gelatinous walls. Plant Physiol. pp.00690.2015. https://doi.org/10.1104/pp.15.00690
497 Greaves, G.N., Greer, A.L., Lakes, R.S., Rouxel, T., 2011. Poisson's ratio and modern materials. Nat.
498 Mater. 10, 823–837. https://doi.org/10.1038/nmat3134
499 Hejnowicz, Z., Sievers, A., 1995. Tissue stresses in organs of herbaceous plants: I. Poisson ratios of
500 tissues and their role in determination of the stresses. J. Exp. Bot. 46, 1035–1043.
501 Kamiya, N., Tazawa, M., Takata, T., 1963. The relation of turgor pressure to cell volume in Nitella with
502 special reference to mechanical properties of the cell wall. Protoplasma 57, 501–521.
503 Kim, K., Yi, H., Zamil, M.S., Haque, M.A., Puri, V.M., 2015. Multiscale stress–strain characterization of
504 onion outer epidermal tissue in wet and dry states. Am. J. Bot. 102, 12–20.
505 https://doi.org/10.3732/ajb.1400273
506 Lehnebach, R., Alméras, T., Clair, B., 2020a. How does bark contribution to postural control change
507 during tree ontogeny? A study of six Amazonian tree species. J. Exp. Bot. 71, 2641–2649.
508 https://doi.org/10.1093/jxb/eraa070
509 Lehnebach, R., Doumerc, L., Clair, B., Alméras, T., 2020b. Mechanical stress in the inner bark of 15
510 tropical tree species and the relationship with anatomical structure. Botany 98, 1–8.
511 https://doi.org/10.1139/cjb-2018-0224
512 Lethbridge, Z.A.D., Walton, R.I., Marmier, A.S.H., Smith, C.W., Evans, K.E., 2010. Elastic anisotropy
513 and extreme Poisson's ratios in single crystals. Acta Mater. 58, 6444–6451.
514 https://doi.org/10.1016/j.actamat.2010.08.006
515 Lockhart, J.A., 1965. An analysis of irreversible plant cell elongation. J. Theor. Biol. 8, 264–275.
516 Masters, I.G., Evans, K.E., 1996. Models for the elastic deformation of honeycombs. Compos. Struct.
517 35, 403–422. https://doi.org/10.1016/S0263-8223(96)00054-2
518 Moulia, B., Coutand, C., Lenne, C., 2006. Posture control and skeletal mechanical acclimation in
519 terrestrial plants: implications for mechanical modeling of plant architecture. Am. J. Bot. 93,
520 1477–1489. https://doi.org/10.3732/ajb.93.10.1477
521 Niklas, K.J., 1999. The mechanical role of bark. Am. J. Bot. 86, 465–469.
522 https://doi.org/10.2307/2656806
523 Niklas, K.J., 1992. Plant Biomechanics : An Engineering Approach to Plant Form and Function.
524 University of Chicago Press.
525 Peel, L.D., 2005. P97 Investigation of High and Negative Poisson's Ratio Laminates, in: Proceedings of
526 the 50th International SAMPE Symposium and Exhibition. Long Beach, CA, USA, p. 14.

527 Rosell, J.A., 2019. Bark in Woody Plants: Understanding the Diversity of a Multifunctional Structure.
528 Integr. Comp. Biol. 59, 535–547. https://doi.org/10.1093/icb/icz057
529 Rosell, J.A., 2016. Bark thickness across the angiosperms: more than just fire. New Phytol. 211, 90–
530 102. https://doi.org/10.1111/nph.13889
531 Rosell, J.A., Olson, M.E., 2014. The evolution of bark mechanics and storage across habitats in a clade
532 of tropical trees. Am. J. Bot. 101, 764–777. https://doi.org/10.3732/ajb.1400109
533 Schneider, C., Rasband, W., Eliceiri, K., 2012. NIH Image to ImageJ: 25 years of image analysis. Nat.
534 Methods 9, 671–675.
535 Scurfield, G., 1973. Reaction Wood: Its Structure and Function. Sci. New Ser. 179, 647–655.
536 Takatera, M., Arichi, T., Peiffer, J., Zhu, C., Kim, K., 2017. Continuous measurement of apparent
537 Poisson's ratio for yarn based on omni-directional diameters. Text. Res. J. 87, 739–746.
538 https://doi.org/10.1177/0040517516639817
539 Videcoq, P., Barbacci, A., Assor, C., Magnenet, V., Arnould, O., Le Gall, S., Lahaye, M., 2017.
540 Examining the contribution of cell wall polysaccharides to the mechanical properties of apple
541 parenchyma tissue using exogenous enzymes. J. Exp. Bot. 68, 5137–5146.
542 https://doi.org/10.1093/jxb/erx329
543 Vu, T.L., Barés, J., Mora, S., Nazamabadi, S., 2019. Deformation Field in Diametrically Loaded Soft
544 Cylinders. Exp. Mech. 59, 453–467. https://doi.org/ref. doi.org/10.1007/s11340-019-00477-4
545 Wang, D., Naouar, N., Vidal-Salle, E., Boisse, P., 2018. Longitudinal compression and Poisson ratio of
546 fiber yarns in meso-scale finite element modeling of composite reinforcements. Compos.
547 Part B Eng. 141, 9–19. https://doi.org/10.1016/j.compositesb.2017.12.042
548 Zajączkowska, U., Kozakiewicz, P., 2016. Interaction between secondary phloem and xylem in
549 gravitropic reaction of lateral branches of Tilia cordata Mill. trees. Holzforschung 70, 993–
550 1002. https://doi.org/10.1515/hf-2015-0230
551
552
553